2005 American Control Conference
June 8-10, 2005. Portland, OR, USA

An Estimation Algorithm for Vision-Based Exploration of Small Bodies in Space

David S. Bayard and Paul B. Brugarolas
Jet Propulsion Laboratory
California Institute of Technology
4800 Oak Grove Drive
Pasadena, CA 91109

***Abstract*— This paper summarizes a methodology for designing on-board state estimators in support of spacecraft exploration of small bodies such as asteroids and comets. This paper will focus on an estimation algorithm that incorporates two basic computer-vision measurement types: a Landmark Table and a Paired Feature Table. Several innovations are developed to incorporate these measurement types into the on-board state estimation algorithm. Simulations are provided to demonstrate the feasibility of the approach.**

I. INTRODUCTION

The exploration of small bodies in space (e.g., asteroids and comets), is emerging as a challenging new area for advanced spacecraft development. Recent missions include the Deep Space 1 mission that flew-by the comet Borrelly [4], the Near Earth Asteroid Rendezvous (NEAR) mission that orbited and eventually landed on the asteroid Eros [13], and the 2004 Stardust mission that flew-through the tail of comet Wild 2 [5]. Challenging on-going missions include the Japanese MUSES-C mission launched in 2003 and scheduled to bring back samples from asteroid 1998SF36 [12], and the Deep Impact mission that is scheduled to drive an impactor at high velocity into comet Temple 1 [11].

Past and current trends indicate that the on-board guidance, navigation and control (GN&C) system for a small body mission will rely heavily on vision-based processing of camera type measurements. In order to help define such a GN&C system, the present paper will focus on developing an estimation algorithm that incorporates two important computer-vision measurement types: the Landmark Table (LMT) and the Paired Feature Table (PFT). The new results reported in this paper first appeared in the engineering document [2].

II. BACKGROUND

The main frames used in the analysis are depicted in Figure 1 and are comprised of the Inertial Frame $\mathcal{F}_I$ located at the Solar System CM (center-of-mass); the Target Body Frame $\mathcal{F}_T$ located at the Target CM; the Spacecraft Body Frame $\mathcal{F}_{sc}$ located at the spacecraft CM; and the Sensor Frame (Camera) $\mathcal{F}_S$ located at the sensor origin.

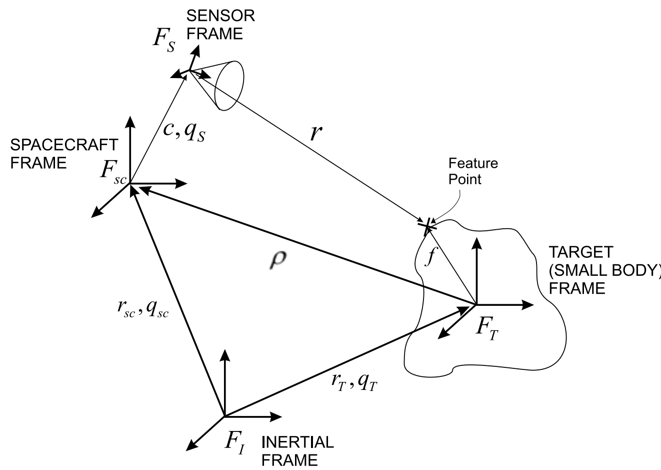

Fig. 1. Frames and Definitions in Small Body Problem

III. ESTIMATION MODEL

The model used for estimator design is given as,

$$\ddot{\rho} = u + \tilde{w} \tag{1}$$

where u is the exogenous (i.e., known) part of the input given by,

$$u = I(t) \cdot a_m - a_T^o + g(r_T^o, \rho^o) \tag{2}$$

and $\tilde{w}$ is the random (i.e., process noise) part of the input given by,

$$\tilde{w} = I(t) \cdot w_a + w_{sc} - w_T + w_g \tag{3}$$

Here, a_m is the accelerometer measurement from the Inertial Measurement Unit (IMU) (m/s^2) with measurement error w_a; w_{sc} and w_T denote unmodeled specific accelerations on the spacecraft and target body, respectively; a_T^o is the nominal (known) specific acceleration of the Target Body; ρ^o and r_T^o denote nominal values of the relative position ρ and target position r_T, respectively; $g(\cdot,\cdot)$ denotes the gravity model used by the estimator; and w_g denotes the unmodeled gravity effects.

$$I(t) \triangleq \begin{cases} 1 & \text{if a thruster is firing} \\ 0 & \text{Otherwise} \end{cases} \tag{4}$$

The need for the function $I(t)$ arises because the accelerometer is only read during periods where the thrusters are known to have fired. This approach desensitizes the estimation results to the degrading effect of accelerometer bias.

The process noise $\tilde{w}$ and its component elements w_a, w_{sc}, w_T, w_g are assumed to be independent zero-mean delta-correlated (white) noise processes with covariances given as,

$$\tilde{Q} \triangleq Cov(\tilde{w}) = \mathit{1}(t) \cdot Q_a + Q_b \quad (5)$$

$$Q_a = Cov(w_a)$$

$$Q_b = Cov(w_{sc} - w_T + w_g) \quad (6)$$

The estimation model can be summarized in state-space notation as,

$$\dot{x} = Ax + \tilde{B}u + \tilde{\Gamma}\tilde{w} \quad (7)$$

where,

$$x = \begin{bmatrix} \rho \\ \dot{\rho} \end{bmatrix}; \; A = \begin{bmatrix} 0 & I \\ 0 & 0 \end{bmatrix}; \; \tilde{B} = \begin{bmatrix} 0 \\ I \end{bmatrix}; \; \tilde{\Gamma} = \begin{bmatrix} 0 \\ I \end{bmatrix} \quad (8)$$

$$\tilde{Q} \triangleq Cov(\tilde{w}) = \mathit{1}(t) \cdot Q_a + Q_b \quad (9)$$

IV. TIME UPDATE

A. Time Discretization

Assuming that $u(t)$ is piecewise constant over each sampling period T, the state-space model (7) can be discretized exactly as,

$$x_{k+1} = Fx_k + \overline{B}u_k + w_k \quad (10)$$

where,

$$F = e^{AT} = \begin{bmatrix} I & T \cdot I \\ 0 & I \end{bmatrix}; \quad \overline{B} = \begin{bmatrix} \frac{T^2}{2} \cdot I \\ T \cdot I \end{bmatrix} \quad (11)$$

$$Cov(w_k) \triangleq Q_k = \begin{bmatrix} \frac{T^3}{3}\tilde{Q} & \frac{T^2}{2}\tilde{Q} \\ \frac{T^2}{2}\tilde{Q} & T \cdot \tilde{Q} \end{bmatrix}; \; \tilde{Q} = \mathit{1}(t) \cdot Q_a + Q_b \quad (12)$$

B. Delay State Augmentation

Since the PFT data type relates states at different times, it will be necessary to "save" certain past states for use at future times. For this purpose, two delayed position states $\rho_{d1} \in \mathcal{R}^3$ and $\rho_{d2} \in \mathcal{R}^3$ will be accommodated by augmenting the state vector with the six additional states,

$$x_{aug} \triangleq \begin{bmatrix} \rho_{d1} \\ \rho_{d2} \end{bmatrix} \quad (13)$$

The total state is denoted as ξ and has the form,

$$\xi \triangleq \begin{bmatrix} x \\ x_{aug} \end{bmatrix} = \begin{bmatrix} \rho_k \\ \dot{\rho}_k \\ \rho_{d1} \\ \rho_{d2} \end{bmatrix} \quad (14)$$

At time t_1 when delay state 1 is to be loaded, the system matrix is put though an additional (artificial) time update of the form,

$$\xi_k(+) = S_1 \xi_k \quad (15)$$

where,

$$S_1 = \begin{bmatrix} I & 0 & 0 & 0 \\ 0 & I & 0 & 0 \\ I & 0 & 0 & 0 \\ 0 & 0 & 0 & I \end{bmatrix} \quad (16)$$

The matrix S_1 acts to set $\rho_{d1} = \rho_k$ at time $t_k = t_1$, but has no effect on any other states.

At the time at which delay state 2 is to be loaded, the system is put through an additional (artificial) time update of the form,

$$\xi_k(+) = S_2 \xi_k \quad (17)$$

where,

$$S_2 = \begin{bmatrix} I & 0 & 0 & 0 \\ 0 & I & 0 & 0 \\ 0 & 0 & I & 0 \\ I & 0 & 0 & 0 \end{bmatrix} \xi_k \quad (18)$$

The matrix S_2 acts to set $\rho_{d2} = \rho_k$ at time $t_k = t_2$, but has no effect on any other states.

For all other times, the delay-states ρ_{d1} and ρ_{d2} are simply held from the previous time, so that the time update becomes,

$$\begin{aligned} \xi_{k+1} &= \begin{bmatrix} F & 0 & 0 \\ 0 & I & 0 \\ 0 & 0 & I \end{bmatrix} \xi_k + \begin{bmatrix} \overline{B} \\ 0 \\ 0 \end{bmatrix} u_k + \begin{bmatrix} I \\ 0 \\ 0 \end{bmatrix} w_k \\ &= \Phi \xi_k + B u_k + \Gamma w_k \end{aligned} \quad (19)$$

Here the top 6 equations are copied from (10), while the remaining bottom equations are chosen simply to hold the delay states without change.

REMARK 1 The need to retain correlations with past states has been recognized earlier by Roumeliotis and Burdick [14] in developing the "stochastic cloning" approach. The method proposed in the present paper is different from stochastic cloning in that the augmented state filter acts as a fixed-point smoother with respect to these delay-states, whereas in stochastic cloning, the updating of past states by subsequent measurements is explicitly prohibited. Consequently, stochastic cloning is suboptimal from an information point of view. Nevertheless, stochastic cloning as practiced in [14] offers some computational savings in being able to generate the correlations analytically without having to explicitly augment the state. ■

C. Kalman Filter Time Update

The Kalman Time Update is of the form,

$$\widehat{\xi}_{k+1|k} = \Phi \widehat{\xi}_{k|k} + B u_k \quad (20)$$

$$M_{k+1} = \Phi P_k \Phi^T + \Gamma Q_k \Gamma^T \quad (21)$$

If time t_k corresponds to a time when delay state 1 is to be loaded (i.e., $t_k = t_1$), an additional artificial time update is used of the form,

$$\widehat{\xi}_k(+) = S_1 \widehat{\xi}_k \quad (22)$$

$$P_k(+) = S_1 P_k S_1^T \quad (23)$$

where S_1 has been defined earlier in (16). If instead, time t_k corresponds to a time when delay state 2 is to be loaded (i.e., $t_k = t_2$), an additional artificial time update is used of the form,

$$\widehat{\xi}_k(+) = S_2 \widehat{\xi}_k \quad (24)$$

$$M_k(+) = S_2 M_k S_2^T \tag{25}$$

where S_2 has been defined earlier in (18).

V. MEASUREMENT UPDATE

A. Landmark Table (LMT) Update

The Landmark Table (LMT) is a table of bearing angles to known landmarks that is provided by the computer vision processing function. Typically, the LMT may contain as many as 50 landmarks. The format of the LMT is shown in Table 1.

Landmark Table (LMT)

#	z_α	z_β	σ_α	σ_β	f^T
1					
$\vdots$					

TABLE I

LANDMARK TABLE (LMT) SPECIFYING BEARING ANGLES TO KNOWN LANDMARKS

In the sensor frame, one can write the following relation between vectors,

$$r = SAT^T f - Sc - SA\rho \tag{26}$$

where r denotes the position vector from the Camera origin to the landmark location on the Target body, resolved in $\mathcal{F}_S$; f denotes the position vector from the Target body CM to the landmark location, resolved in $\mathcal{F}_T$; c denotes the position vector from the Spacecraft CM to the Camera origin, resolved in $\mathcal{F}_{sc}$; A is the spacecraft attitude as a DCOS matrix; S is the Spacecraft-to-Camera transformation as a DCOS matrix; and T is the Target attitude as a DCOS matrix.

Equation (26) can be rewritten as,

$$r = \overline{d} - SA\rho \tag{27}$$

where $\overline{d}$ is the fixed offset vector,

$$\overline{d} \triangleq SAT^T f - Sc \tag{28}$$

Each row of the LMT contains camera measurements z_α, z_β which are defined as the projections of r into the camera frame. Specifically,

$$z_\alpha \triangleq tan(\alpha) = r_y / r_x \tag{29}$$

$$z_\beta \triangleq tan(\beta) = r_z / r_x \tag{30}$$

where,

$$r = \begin{bmatrix} r_x \\ r_y \\ r_z \end{bmatrix} \tag{31}$$

The camera information from a single landmark (i.e., one row of the LMT) can be written as,

$$y = \begin{bmatrix} z_\alpha \\ z_\beta \end{bmatrix} + \begin{bmatrix} n_\alpha \\ n_\beta \end{bmatrix} \tag{32}$$

$$Cov[n_\alpha] = \sigma_\alpha^2; \quad Cov[n_\beta] = \sigma_\beta^2 \tag{33}$$

where n_α and n_β are independent noises associated with the camera measurement.

In order to develop a linearized measurement, the sensitivity equations are computed as,

$$Z_\alpha \triangleq \frac{\partial z_\alpha}{\partial \rho} = \left[\frac{\partial z_\alpha}{\partial r}\right]\left[\frac{\partial r}{\partial \rho}\right] = \frac{1}{r_x^2}[r_y, \; -r_x, \; 0]\, SA \tag{34}$$

$$Z_\beta \triangleq \frac{\partial z_\beta}{\partial \rho} = \left[\frac{\partial z_\beta}{\partial r}\right]\left[\frac{\partial r}{\partial \rho}\right] = \frac{1}{r_x^2}[r_z, \; 0, \; -r_x]\, SA \tag{35}$$

Let ρ^o denote a nominal value of the relative position vector, and consider the first-order expansion,

$$y = y^o + H(\rho - \rho^o) + n \tag{36}$$

where,

$$y^o \triangleq \begin{bmatrix} z_\alpha(\rho^o) \\ z_\beta(\rho^o) \end{bmatrix}; \quad H \triangleq \begin{bmatrix} Z_\alpha(\rho^o) \\ Z_\beta(\rho^o) \end{bmatrix} \tag{37}$$

$$n = \begin{bmatrix} n_\alpha \\ n_\beta \end{bmatrix}; \quad N \triangleq Cov[n] = \begin{bmatrix} \sigma_\alpha^2 & 0 \\ 0 & \sigma_\beta^2 \end{bmatrix} \tag{38}$$

Rearranging (36) gives the desired linear measurement equation in the relative position ρ,

$$\delta y \triangleq y - y^o + H\rho^o = H\rho + n \tag{39}$$

These rows are then noise-normalized by multiplying on the left by $N^{-\frac{1}{2}} = diag[\frac{1}{\sigma_\alpha}, \frac{1}{\sigma_\beta}]$ to give,

$$\delta\tilde{y} = \tilde{H}\rho + \tilde{n} \tag{40}$$

where,

$$\delta\tilde{y} = N^{-\frac{1}{2}}\delta y; \quad \tilde{H} = N^{-\frac{1}{2}} H \tag{41}$$

$$\tilde{n} = N^{-\frac{1}{2}} n; \quad Cov[\tilde{n}] = I \tag{42}$$

It is convenient to index each of these 2×1 measurements by j (corresponding to the j'th row of the LMT), so that (40) is replaced with,

$$\delta\tilde{y}_j = \tilde{H}_j \rho + \tilde{n}_j, \quad j = 1, ..., N \tag{43}$$

The noise-normalized equations (43) are then stacked into a single tall measurement update of the form,

$$Y_{stack} = H_{stack}\ \rho + n_{stack} \tag{44}$$

where,

$$Y_{stack} = \begin{bmatrix} \delta\tilde{y}_1 \\ \vdots \\ \delta\tilde{y}_N \end{bmatrix}; \quad H_{stack} = \begin{bmatrix} \tilde{H}_1 \\ \vdots \\ \tilde{H}_N \end{bmatrix} \tag{45}$$

$$n_{stack} = \begin{bmatrix} \tilde{n}_1 \\ \vdots \\ \tilde{n}_N \end{bmatrix}; \quad Cov[n_{stack}] = I \tag{46}$$

A pre-processing step will now be introduced that uses a QR factorization to improve numerical robustness, and to reduce overall in-flight computation. Specifically, a QR decomposition of H_{stack} is taken of the form,

$$H_{stack} = QR = [Q_1, Q_2]\begin{bmatrix} R_{11} \\ 0 \end{bmatrix} = Q_1 R_{11} \tag{47}$$

where $R_{11} \in R^{3\times 3}$. Multiplying (44) on the left by Q^T and using (47) gives the equivalent measurement equation,

$$Q^T Y_{stack} = \begin{bmatrix} R_{11} \\ 0 \end{bmatrix}\rho + Q^T n_{stack} \tag{48}$$

A key observation is that all but the top 3 equations of (48) are pure noise and can be removed from consideration. Keeping only the top 3 equations of (48) gives,

$$y_3 = R_{11}\rho + n_3 \tag{49}$$

where,

$$y_3 = Q_1^T Y_{stack}; \quad n_3 = Q_1^T n_{stack} \tag{50}$$

$$R_3 = Cov[n_3] = I \tag{51}$$

REMARK 2 Using a well-known method, additional computation can be saved by not forming Q_1 explicitly, but rather, augmenting H_{stack} on the right with Y_{stack} before taking the QR factorization in (47)(cf., [16]). ■

REMARK 3 If the stacked measurement (44) were used directly in a KF update, it would involve inversion of an $N \times N$ matrix. This step alone requires approximately N^3 flops, which is prohibitive for large N (say $N = 50$). Alternatively, because the noise covariance is diagonal (i.e., $Cov[n_{stack}] = I$), the measurements can be applied as scalar updates. When carefully arranged (see Bierman's approach [3]), scalar updates can reduce the computation to approximately $\frac{9}{2}Nn^2$ flops (where n is the number of states and N the number of measurements), which amounts to considerable savings when $N >> n$. The proposed QR-factorization approach has further computational savings and other advantages relative to scalar updates that are now discussed.

Equation (49) is equivalent to the stacked measurement equation (44) but has been heavily compressed into only 3 equations. It can be shown [2] that this QR-based pre-processing stage is equivalent to using an information filter to compress the data in the LMT, but with the additional advantages of (1) computation on the order of $\frac{1}{2}Nn^2$ which is almost an order of magnitude reduced compared to scalar updates; (2) not squaring the condition number of H_{stack}; (3) avoiding an unnecessary matrix inversion of R_{11}, and (4) keeping the noise covariance R_3 an identity matrix, to allow arbitrary (e.g., scalar) updates. This particular use of QR factorization for pre-processing appears to be new and very useful. However it is closely related to existing approaches for applying QR methods (and more generally, unitary triangularization) to least-squares problems [8] and square-root filtering problems [1][10]. ■

The algorithm checks the size of the elements in each row of R_{11} (an upper triangular matrix) to see whether 1, 2, or 3 of the measurements in (49) should be applied for KF updating. They can then be applied as scalar updates, or in a single update (requiring the KF to invert at most a 3×3 matrix).

One can write ρ as,

$$\rho = [I, 0, 0, 0]\xi \tag{52}$$

Substituting (52) into (49) gives the final measurement equation of the form,

$$y_3 = H_3\xi + n_3 \tag{53}$$

where,

$$H_3 = R_{11}[I, 0, 0, 0] \tag{54}$$

B. Paired Feature Table (PFT) Update

The format of the PFT is shown in Table 2. Consider a first image I_1 taken at time t_1 and a second image I_2 taken at time t_2. The bearing angles to each feature recognized as being common to the images I_1 and I_2 are reported in a separate row in the PFT. Typically, the PFT may contain as many as 50 feature points. Unlike the LMT, the feature's physical location on the target body is not required for generating the PFT.

Paired Feature Table (PFT)

#	$z_{\alpha 2}$	$z_{\beta 2}$	$\sigma_{\alpha 2}$	$\sigma_{\beta 2}$	$z_{\alpha 1}$	$z_{\beta 1}$	$\sigma_{\alpha 1}$	$\sigma_{\beta 1}$
1								
$\vdots$								

TABLE 2

PAIRED FEATURE TABLE (PFT) SPECIFYING BEARING ANGLES TO FEATURES COMMON TO TWO IMAGES

At time t_1 one can write the following relation between vectors in the sensor frame,

$$r_1 = SA_1T_1^T f - Sc - SA_1\rho_1 \tag{55}$$

where r_1, A_1, T_1 correspond to r, A, T defined earlier in Section V-A, but sampled at time t_1.

Each row of the PFT contains camera measurements $z_{\alpha 1}, z_{\beta 1}$ taken at time t_1 which are ideally defined as the projections of r_1 into the camera frame. Specifically,

$$z_{\alpha 1} = tan(\alpha 1) = r_{1y}/r_{1x} \tag{56}$$

$$z_{\beta 1} = tan(\beta 1) = r_{1z}/r_{1x} \tag{57}$$

where,

$$r_1 \triangleq \begin{bmatrix} r_{1x} \\ r_{1y} \\ r_{1z} \end{bmatrix} = \begin{bmatrix} 1 \\ r_{1y}/r_{1x} \\ r_{1z}/r_{1x} \end{bmatrix} r_{1x} = \begin{bmatrix} 1 \\ z_{\alpha 1} \\ z_{\beta 1} \end{bmatrix} r_{1x} \tag{58}$$

Solving for f in (55) and using the relation (58) gives,

$$\begin{aligned} f &= T_1A_1^TS^Tr_1 + T_1A_1^Tc + T_1\rho_1 \\ &= T_1A_1^TS^T \begin{bmatrix} 1 \\ z_{\alpha 1} \\ z_{\beta 1} \end{bmatrix} r_{1x} + T_1A_1^Tc + T_1\rho_1 \end{aligned} \tag{59}$$

Likewise, at time t_2 one can write the following relation in the sensor frame,

$$r_2 = SA_2T_2^T f - Sc - SA_2\rho_2 \tag{60}$$

where r_2, A_2, T_2 correspond to r, A, T defined earlier in Section V-A, but sampled at time t_2.

Each row of the PFT contains camera measurements $z_{\alpha 2}, z_{\beta 2}$ taken at time t_2 which are ideally defined as the projections of r_2 into the camera frame. Specifically,

$$z_{\alpha 2} = tan(\alpha 2) = r_{2y}/r_{2x} \tag{61}$$

$$z_{\beta 2} = tan(\beta 2) = r_{2z}/r_{2x} \tag{62}$$

where,

$$r_2 \triangleq \begin{bmatrix} r_{2x} \\ r_{2y} \\ r_{2z} \end{bmatrix} = \begin{bmatrix} 1 \\ r_{2y}/r_{2x} \\ r_{2z}/r_{2x} \end{bmatrix} r_{2x} = \begin{bmatrix} 1 \\ z_{\alpha 2} \\ z_{\beta 2} \end{bmatrix} r_{2x} \tag{63}$$

Solving for f in (60) and using the relation (63) gives,

$$\begin{aligned} f &= T_2 A_2^T S^T r_2 + T_2 A_2^T c + T_2 \rho_2 \\ &= T_2 A_2^T S^T \begin{bmatrix} 1 \\ z_{\alpha 2} \\ z_{\beta 2} \end{bmatrix} r_{2x} + T_2 A_2^T c + T_2 \rho_2 \end{aligned} \quad (64)$$

Since the same feature on the target body is common to both images, one can equate (59) and (64) to give the desired relation, denoted as the "Invariant Equation",

Invariant Equation

$$\begin{aligned} T_2 A_2^T S^T \begin{bmatrix} 1 \\ z_{\alpha 2} \\ z_{\beta 2} \end{bmatrix} r_{2x} + T_2 A_2^T c + T_2 \rho_2 = f \\ = T_1 A_1^T S^T \begin{bmatrix} 1 \\ z_{\alpha 1} \\ z_{\beta 1} \end{bmatrix} r_{1x} + T_1 A_1^T c + T_1 \rho_1 \end{aligned} \quad (65)$$

Even though f is unknown in the Invariant Equation, it does not cause a problem because it can be eliminated by rearranging (65) to become,

$$T_2 \rho_2 - T_1 \rho_1 = [h_1, h_2] \begin{bmatrix} r_{1x} \\ r_{2x} \end{bmatrix} + (T_1 A_1^T c - T_2 A_2^T c) \quad (66)$$

where,

$$h_1 = T_1 A_1^T S^T \begin{bmatrix} 1 \\ z_{\alpha 1} \\ z_{\beta 1} \end{bmatrix}; \quad h_2 = -T_2 A_2^T S^T \begin{bmatrix} 1 \\ z_{\alpha 2} \\ z_{\beta 2} \end{bmatrix} \quad (67)$$

It will be convenient to define the notation,

$$D\, \overline{x} = T_2 \rho_2 - T_1 \rho_1 \quad (68)$$

where,

$$D = [T_2, -T_1]; \quad \overline{x} = \begin{bmatrix} \rho_2 \\ \rho_1 \end{bmatrix} \quad (69)$$

The quantity $\overline{x}$ serves as a reduced state vector containing only the delay-states. With this notation, equation (66) can be rearranged to give,

$$D\, \overline{x} = H \begin{bmatrix} r_{1x} \\ r_{2x} \end{bmatrix} + \tilde{c} \quad (70)$$

where,

$$H = [h_1, h_2]; \quad \tilde{c} = (T_1 A_1^T c - T_2 A_2^T c) \quad (71)$$

REMARK 4 Unfortunately, it is impossible to use (70) as a measurement equation because the quantities r_{1x} and r_{2x} are unknown, i.e., they are associated with a feature having an unknown location. The remainder of this section is directed at mitigating this problem. Note that this difficulty does not arise in reference [14] because that paper assumes a measurement of the full Cartesian difference (equivalent to $y = \rho_2 - \rho_1$), rather than just the bearing angles. ■

At this point, a QR factorization of H is performed to give,

$$H = Q_1 R_{11} \quad (72)$$

where,

$$Q_1 = [q_1, q_2] \in R^{3\times 2}; \quad R_{11} \in R^{2\times 2} \quad (73)$$

Since q_1 and q_2 are orthogonal and in R^3, one can complete the triad by forming q_3 where,

$$q_3 \triangleq q_1 \times q_2 \quad (74)$$

It is noted that q_3 is a left annihilator of H since by construction $q_3^T Q_1 = 0$ and hence,

$$q_3^T H = q_3^T Q_1 R_{11} = 0 \quad (75)$$

This special property will now be used to advantage. Equation (70) can be left multiplied by q_3 to give,

$$q_3^T D \overline{x} = q_3^T H \begin{bmatrix} r_{1x} \\ r_{2x} \end{bmatrix} + q_3^T \tilde{c} \quad (76)$$

Applying the annihilation condition (75) to (76) gives the simplified expression,

$$q_3^T \tilde{c} = q_3^T D \overline{x} \quad (77)$$

This serves as the desired measurement equation, since the right hand side is a linear function of the reduced state $\overline{x}$.

REMARK 5 It is emphasized that the annihilation property $q_3^T H = 0$ was invoked here to remove the dependence of (76) on the unavailable quantities r_{1x}, r_{2x}. This led directly to the desired linear measurement equation (77) for the PFT update. The use of an annihilator in this fashion is a novel aspect of the present research. However, the idea is not completely original, being closely related to the notion of the "epipolar constraint" found in the computer vision literature [6]. ■

Interestingly, if R_{11} is singular, an additional measurement relation can be derived. Due to space constraints, the reader is referred to [2] for details.

The resulting measurement equations are then noise-normalized, stacked, and then pre-processed using a QR-factorization step analogous to the one used previously for the LMT update. It has been found empirically that only the top 3 rows of the resulting compressed measurement equation contribute significantly and need to be used for the KF update.

C. Kalman Filter Measurement Update

The LMT and PFT data types lead to measurement equations of the general form,

$$y_k = H_k \xi_k + n_k \quad (78)$$

$$Cov[n_k] = R_k \quad (79)$$

Given measurements of this form, the Kalman filter measurement update has the general form (cf., [7]),

$$\widehat{\xi}_{k|k} = \widehat{\xi}_{k|k-1} + K_k (y_k - H_k \widehat{\xi}_{k|k-1}) \quad (80)$$

$$K_k = M_k H_k^T \Big((1 + \mathtt{uw}) H_k M_k H_k^T + R_k \Big)^{-1} \quad (81)$$

$$P_k = (I - K_k H_k) M_k (I - K_k H_k)^T + K_k R_k K_k^T \quad (82)$$

The use of an underweighting factor $\mathtt{uw} > 0$ is inherited from the NASA Apollo program, and is used to intentionally slow adaptation in linearized estimation problems. The use of Joseph's form in (82) ensures that the covariances will still be propagated correctly using the associated reduced estimator gains [7].

VI. EXAMPLES

A fly-around scenario is shown in Figure 2. Here, a 5 hour scenario is shown where the spacecraft takes 1 hour to get into position, and then flies a 4-hour forced trajectory, using thrusters, around the small body. The accelerometer has a 40 ug bias error, a velocity random walk of $Q_a = 1e-6 \cdot I \ \ (m^2/s^3)$, and the unmodelled accelerations are simulated with covariance $Q_b = 1e-6 \cdot I \ \ (m^2/s^3)$. The estimator is given a 500 meter initial position error, and a 50 (cm/sec) initial velocity error.

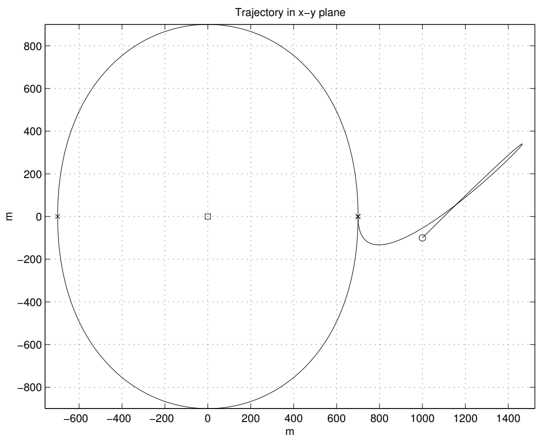

Fig. 2. Fly-around trajectory for estimator study

A. Case Study: Landmark Table (LMT) Measurement

The LMT is generated by assuming that a set of 4 landmarks separated by approximately 80 meters is visible to, and recognized by the camera at all times. The camera accuracy in computing bearing angles is assumed to be 1/20 degree, 1-sigma, and an underweighting factor of $\mathtt{uw} = 5$ is used for all measurement updates.

The true and estimated position, and the errors between them, are shown in Figure 3 and Figure 4 respectively. The true and estimated velocity, and the errors between them, are shown in Figure 5, and Figure 6, respectively. All estimation errors agree with their expected 1-sigma bounds. The position converges to about 2-3 meters error, and the velocity converges to about 2-3 cm/sec error. The position transient converges in about 50 seconds while the velocity transient takes longer and converges in about 300 seconds.

B. Case Study: Paired Feature Table (PFT) Measurement

The PFT is generated by assuming that a set of 8 landmarks separated by approximately 80 meters is visible to, and recognized by the camera in all images. The camera accuracy in measuring bearing angles is assumed to be 1/20 degree, 1-sigma, and an underweighting factor of $\mathtt{uw} = 5$ is used for all measurement updates. The PFT measurements are generated once every 2 minutes.

The true and estimated velocity, and the errors between them, are shown in Figure 7 and Figure 8, respectively. It is seen that the estimation errors agree with their expected

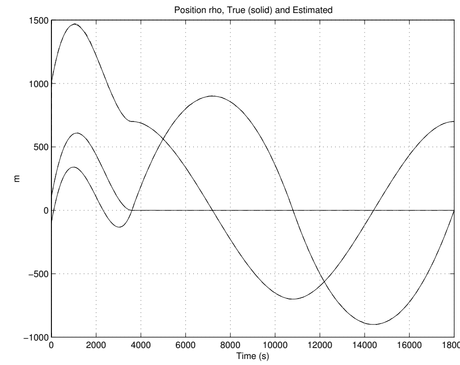

Fig. 3. True (solid) and estimated (dashed) position using LMT

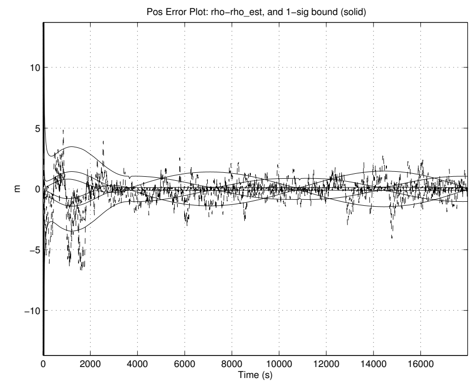

Fig. 4. Position error (dash) and 1-sigma bound (solid) using LMT

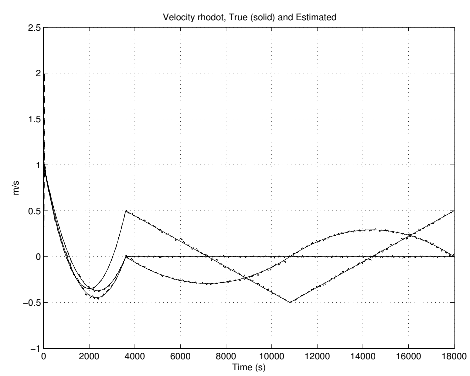

Fig. 5. True (solid) and estimated (dashed) velocity using LMT

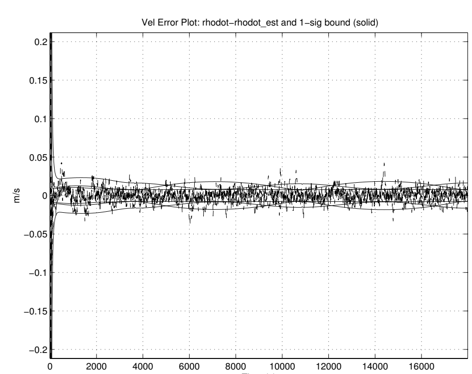

Fig. 6. Velocity error (dash) and 1-sigma bound (solid) using LMT

1-sigma bounds. The velocity error converges in about 3000 seconds. The PFT update is important because it keeps the velocity error from growing in an unbounded fashion due to the bias in the accelerometer.

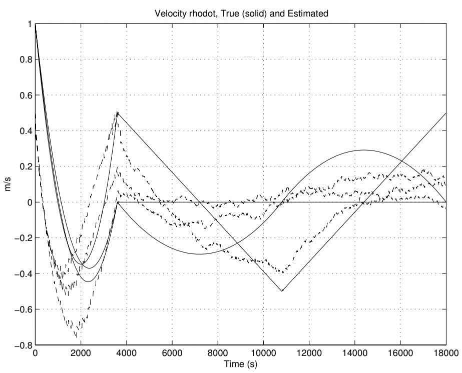

Fig. 7. True (solid) and estimated (dashed) velocity using PFT

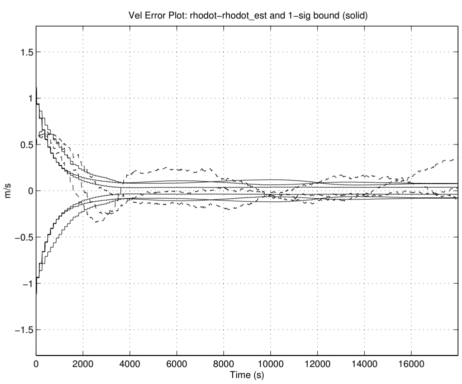

Fig. 8. Velocity error (dash) and 1-sigma bound (solid) using PFT

VII. CONCLUSIONS

It is shown that an on-board state estimator can be designed that accepts both LMT and PFT type measurement updates obtained from real-time vision-based processing of images. Such measurement types are central to camera-based approaches for exploration of small bodies. Several new algorithmic innovations were introduced to accommodate these highly specialized vision-based measurement types, including a pre-processing step based on QR factorization (to optimally compress LMT and PFT updates having large numbers of recognized features), an annihilation method to form a linear measurement equation from the PFT data type, and a state augmentation method to handle measurements (e.g., of the PFT type), that relate states from different time instants. The estimation algorithm has been shown by simulation to perform as expected, with the LMT updates providing good position type information, and the PFT updates providing useful velocity type information.

Future research will concentrate on accommodating landmark location errors in the LMT definition, and on handling potential uncertainty in the data associations made in constructing both the LMT and PFT.

VIII. ACKNOWLEDGEMENTS

The authors would like to thank Dr. Adnan Ansar, Dr. Andrew Johnson, and Dr. Curtis Padgett of JPL for several technical discussions on camera capabilities and models. This research was performed at the Jet Propulsion Laboratory, California Institute of Technology, under contract with the National Aeronautics and Space Administration, and funded through the internal Research and Technology Development program.

REFERENCES

[1] B.D.O. Anderson and J.B. Moore, *Optimal Filtering.* Prentice-Hall, Englewood Cliffs, New Jersey, 1979.

[2] D.S. Bayard and P.B. Brugarolas, *Small Body GN&C Research Report: Estimation Algorithms.*, Internal Document, JPL D-30281, September 24, 2004.

[3] G.J. Bierman, *Factorization Methods for Discrete Sequential Estimation*. Academic Press, San Diego, 1977.

[4] S. Bhaskaran, J.E. Riedel, B.M. Kennedy, T.C. Wang, "Navigation of the Deep Space 1 Spacecraft at Borrelly," Paper AIAA 2002-4815, AIAA/AAS Astrodynamics Specialists Conference, Monterey, California, August 5-8, 2002.

[5] S. Bhaskaran, J.E. Riedel, S.P. Synnott, "Autonomous Nucleus Tracking for Comet/Asteroid Encounters: The STARDUST Example," IEEE Aerospace Conference Proceedings, Vol 2, pp. 353-365, March 21-28, 1998.

[6] O. Faugeras, *Three-Dimensional Computer Vision: A Geometric Viewpoint*, The MIT Press, Cambridge, Massachusetts, 2001.

[7] A. Gelb (Ed.), *Applied Optimal Estimation.* The MIT Press, Cambridge, Massachusetts, 1984.

[8] G.H. Golub and C.F. Van Loan, *Matrix Computations*. The John Hopkins University Press, Baltimore, Maryland, 1983.

[9] R. Hashimoto, T. Kubota, J. Kawaguchi, M. Uo, K. Baba, T. Yamashita, "Autonomous Descent and Touch-Down via Optical Sensors," Paper AAS 01-134, AAS/AIAA Space Flight Mechanics Meeting, Santa Barbara, California, February 11-14, 2001.

[10] T. Kailath, A.H. Sayed, and B. Hassibi, *Linear Estimation*. Prentice Hall, Upper Saddle River, New Jersey, 2000.

[11] D.G. Kubitschek, "Impactor Spacecraft Targeting for the Deep Impact Mission to Comet Tempel 1," Paper AAS 03-615, AAS/AIAA Astrodynamics Specialists Conference, Big Sky Resort, Big Sky, Montana, August 3-7, 2003.

[12] T. Kubota, T. Hashimoto, J. Kawaguchi, "Image Processing for Asteroid Exploration Mission MUSES-C," Proc. ICAR 2003, 11'th International Conference on Advanced Robotics, Coimbra, Portugal, June 30 - July 3, 2003.

[13] W.M. Owen, T.C. Wang, "NEAR Optical Navigation at Eros," Paper AAS 01-376, AAS/AIAA Astrodynamics Specialists Conference, Quebec City, Quebec, Canada, July 30-August 2, 2001.

[14] S.I. Roumeliotis and J.W. Burdick, "Stochastic Cloning: A Generalized Framework for Processing Relative State Measurements," Proc. 2002 IEEE International Conference on Robotics & Automation, Washington DC, May 2002.

[15] S.I. Roumeliotis, A.E. Johnson, and J.F. Montgomery, "Augmenting Inertial Navigation with Image-Based Motion Estimation," Proc. 2002 IEEE International Conference on Robotics & Automation, Washington, DC, May 2002.

[16] L.N. Trefethen and D. Bau, *Numerical Linear Algebra*, Society for Industrial and Applied Mathematics, Philadelphia, PA, 1977.